Virology 458-459 (2014) 125–135

Contents lists available at ScienceDirect

Virology

journal homepage: www.elsevier.com/locate/yviro

Membrane rearrangements mediated by coronavirus nonstructural proteins 3 and 4

Marne C. Hagemeijer [a,1], Iryna Monastyrska [a], Janice Griffith [b], Peter van der Sluijs [b], Jarno Voortman [c], Paul M. van Bergen en Henegouwen [c], Annelotte M. Vonk [a], Peter J.M. Rottier [a], Fulvio Reggiori [b], Cornelis A.M. de Haan [a,*]

[a] Virology Division, Department of Infectious Diseases & Immunology, Faculty of Veterinary Medicine, Utrecht University, Yalelaan 1, 3584 CL Utrecht, The Netherlands
[b] Department of Cell Biology and Institute of Biomembranes, University Medical Centre Utrecht, Utrecht, The Netherlands
[c] Division of Cell Biology, Department of Biology, Science Faculty, Utrecht University, Utrecht, The Netherlands

ARTICLE INFO

Article history:
Received 9 February 2014
Returned to author for revisions
26 February 2014
Accepted 22 April 2014
Available online 13 May 2014

Keywords:
Coronavirus
Nsps
Replication–transcription complex
Transmembrane proteins
Membrane rearrangements

ABSTRACT

Coronaviruses replicate their genomes in association with rearranged cellular membranes. The coronavirus nonstructural integral membrane proteins (nsps) 3, 4 and 6, are key players in the formation of the rearranged membranes. Previously, we demonstrated that nsp3 and nsp4 interact and that their co-expression results in the relocalization of these proteins from the endoplasmic reticulum (ER) into discrete perinuclear foci. We now show that these foci correspond to areas of rearranged ER-derived membranes, which display increased membrane curvature. These structures, which were able to recruit other nsps, were only detected when nsp3 and nsp4 were derived from the same coronavirus species. We propose, based on the analysis of a large number of nsp3 and nsp4 mutants, that interaction between the large luminal loops of these proteins drives the formation of membrane rearrangements, onto which the coronavirus replication–transcription complexes assemble in infected cells.

Introduction

One of the hallmarks of positive-strand RNA (+RNA) viruses is the induction of membranous rearrangements of varying morphologies that serve as platforms for the viral replication and transcription complexes (RTCs) that are intimately associated with them [reviewed in Miller and Krijnse-Locker (2008, den Boon and Ahlquist (2010a), den Boon et al. (2010b), Delang et al. (2012)]. Assembly of the viral RTCs on host-derived membranes provides a dual advantage for the virus by (i) ensuring that cellular and viral constituents required for RNA synthesis are optimally spatio-temporally organized and by (ii) concealing the multiple viral RNA species generated during viral replication from the anti-viral host defense mechanisms of the infected cell. It is becoming apparent that the generation of these replication platforms depends on the concerted actions of hijacked host and viral membrane-shaping proteins, lipid-modifying enzymes and various exploited cellular pathways [reviewed in Miller and Krijnse-Locker (2008), den Boon and Ahlquist (2010a), den Boon et al. (2010b), Altan-Bonnet and Balla (2012), Belov and van Kuppeveld (2012), Delang et al. (2012), Hagemeijer et al. (2012a)].

Coronaviruses (CoVs) are enveloped +RNA viruses that belong to the family *Coronaviridae* in the order of the *Nidovirales*. The CoV-induced replicative structures consist of double-membrane vesicles (DMVs) and convoluted membranes (CMs) (Gosert et al., 2002; Goldsmith et al., 2004; Snijder et al., 2006; Ulasli et al., 2010), which form an interconnected reticulovesicular network of modified membranes that appears to be continuous with the endoplasmic reticulum (ER) (Knoops et al., 2008; Hagemeijer et al., 2011), as has been observed in cells infected with severe acute respiratory syndrome (SARS)-CoV or mouse hepatitis virus (MHV). Similar structures have also been observed for the recently emerged Middle East respiratory syndrome (MERS)-CoV (de Wilde et al., 2013). Recently Maier et al. demonstrated that in addition to DMVs and CMs, the avian CoV infectious bronchitis virus (IBV) induces small double-membrane spherule-like structures that are associated with zippered ER membranes (Maier et al., 2013). These structures have not been observed however in SARS-CoV, MHV- or MERS-CoV-infected cells. Replication-associated viral proteins have been demonstrated to localize both the DMVs and CMs (Shi et al., 1999; van der Meer et al., 1999; Goldsmith et al., 2004; Prentice et al., 2004; Graham et al., 2005; Snijder et al., 2006; Deming et al., 2007; Oostra et al., 2007; Knoops et al., 2008;

* Corresponding author. Tel.: +31 30 2534195; fax: +31 30 2536723.
E-mail address: c.a.m.dehaan@uu.nl (C.A.M. de Haan).
[1] Present address: Laboratory of Host-Pathogen Dynamics, Cell Biology and Physiology Center (CBPC), National Heart Lung and Blood Institute (NHLBI), National Institutes of Health, Bethesda, MD, USA.

http://dx.doi.org/10.1016/j.virol.2014.04.027
0042-6822/

Reggiori et al., 2010; Ulasli et al., 2010) whereas double-stranded RNA (dsRNA) – presumably (once) functioning as replicative intermediate during viral RNA synthesis – has been detected in the interior of the DMVs (Knoops et al., 2008). Early in infection, viral proteins and nascent RNAs colocalize with or occur adjacent to dsRNA puncta, whereas the correlation between these different molecules is less obvious late in infection (Hagemeijer et al., 2012b). It has recently been proposed that CoVs hijack EDEMosomes, ER-derived vesicles involved in the transport of selected short-lived ER chaperones to the endosomal system, to generate the CoV replicative structures (Reggiori et al., 2010; Bernasconi et al., 2012).

When compared to other +RNA viruses, CoVs possess extremely large genomes that range in size from ~26 to 32 kb (Gorbalenya et al., 2006). Two-thirds of the genome encodes the nonstructural proteins (nsps), which together with the nucleocapsid (N) protein, and presumably host proteins, form the membrane-associated RTCs (Shi et al., 1999; van der Meer et al., 1999; Goldsmith et al., 2004; Prentice et al., 2004, Graham et al., 2005; Snijder et al., 2006; Deming et al., 2007; Oostra et al., 2007; Knoops et al., 2008; Reggiori et al., 2010; Ulasli et al., 2010; Verheije et al., 2010). Among the 16 nsps, three contain multiple hydrophobic, membrane-spanning domains: nsp3, nsp4 and nsp6 (Harcourt et al., 2004; Kanjanahaluethai et al., 2007; Oostra et al., 2007; Oostra et al., 2008; Baliji et al., 2009). Recently, Angelini et al. showed that co-expression of full-length nsp3, nsp4 and nsp6 resulted in the formation of CMs and DMVs that resemble to some extent the replicative structures as have been observed in infected cells (Angelini et al., 2013). We previously demonstrated that the membrane-spanning nsps are involved in homo- and heterotypic interactions using co-immunoprecipitation (coIP) and protein complementation assays (Hagemeijer et al., 2011). Furthermore we showed that co-expression of nsp4 with the C-terminal one-third part of nsp3 ($nsp3_C$), which contains the transmembrane domains, redistributes both proteins from the ER into discrete foci that predominantly localize in the perinuclear region of the cell (Hagemeijer et al., 2011). Together these results indicate an important role for the integral membrane nsps in the induction of the CoV replicative structures. In agreement herewith, Sparks et al. have demonstrated that nsp4 is essential for CoV replication (Sparks et al., 2007) and that disruption of the nsp4 glycosylation sites present in the large luminal loop between the first and second transmembrane domain gives rise to aberrant DMVs with detached inner and outer membranes and to a concomitant increased number of CMs (Gadlage et al., 2010).

In view of the importance of the membrane-spanning nsps in CoV replication and the formation of organelle-like replicative structures, we decided to characterize and study the role of these proteins in the induction of membrane rearrangements in more detail, thereby focusing on the membrane rearrangements induced by the co-expression of $nsp3_C$ and nsp4 (see Fig. 1A for a representation of the membrane structure of these proteins). Our results indicate that the foci induced by co-expression of $nsp3_C$ and nsp4 correspond with ER-derived membranes that display increased membrane curvature and resemble the recently described areas of maze-like bodies (MLBs) (Angelini et al., 2013). Importantly, these membrane rearrangements were only observed when the co-expressed $nsp3_C$ and nsp4 proteins were derived from the same CoV species. The specific interplay between the two proteins was attributed to the large luminal loops of nsp3 and nsp4. In agreement herewith, mutation of the conserved cysteine residues in the loop of nsp4 completely abrogated the formation of membrane rearrangements. Finally, we show that the foci induced by co-expression of $nsp3_C$ and nsp4 were able to recruit nsp2 and nsp6 in agreement with the idea that the integral membrane proteins not only function in the biogenesis of the membranous rearrangements, but also in the anchoring of other nsps, onto what will eventually become the replicative structures.

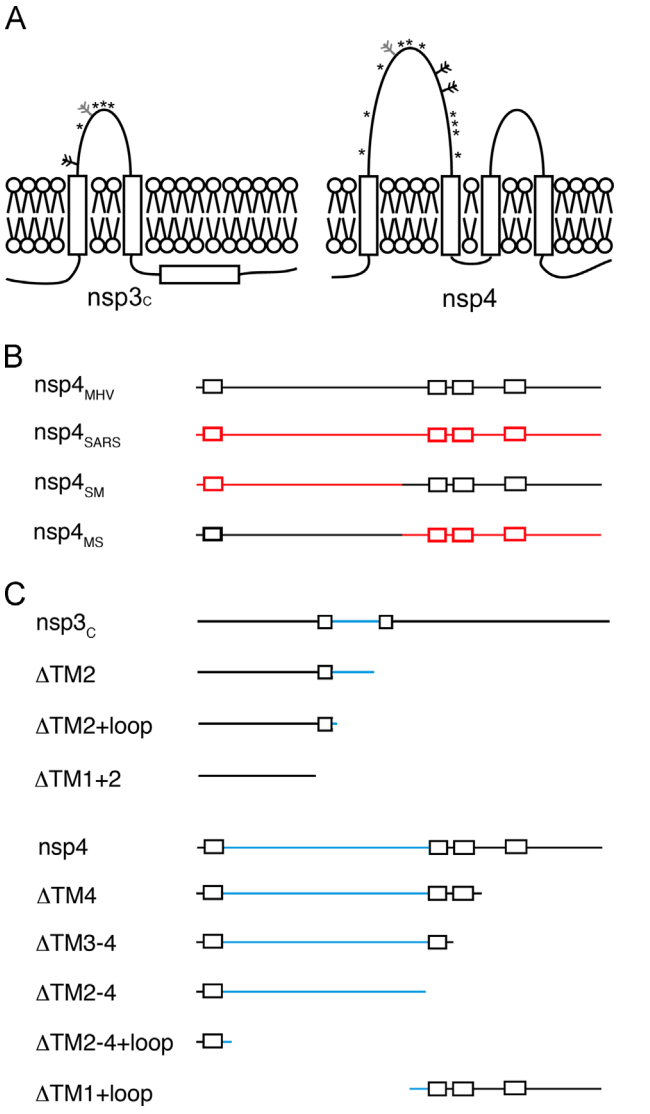

Fig. 1. Overview of CoV $nsp3_C$ and nsp4 constructs used in this study. (A) A schematic representation of the membrane topology of the C-terminal part of nsp3 ($nsp3_C$), and of nsp4. The approximate location of the cysteine residues (*) and *N*-glycosylation sites (-«) in the large luminal loops are indicated, the latter either in gray (SARS-CoV) or in black (MHV-A59). (B) Schematic representation of nsp4 hybrid proteins. Nsp4 sequences derived from MHV or SARS-CoV are indicated by black (MHV) or red (SARS-CoV) lines or rectangles. Rectangles indicate the approximate location of transmembrane domains. $Nsp4_{SM}$ contains the amino-terminal half of SARS-CoV, while its carboxy terminus is derived from MHV. $Nsp4_{MS}$ refers to the reciprocal hybrid protein. (C) Schematic representation of the MHV nsp3 and nsp4 deletion mutants used in this study. Rectangles indicate transmembrane domains and the blue lines indicate either the luminal loop of nsp3 or the large luminal loop of nsp4.

Results

Co-expression of $nsp3_C$ and nsp4 induces ER membrane rearrangements

We have previously shown that $nsp3_C$ and nsp4, which localize to the ER when expressed individually, interact with each other and that their co-expression results in the relocalization of these proteins from the ER to discrete foci mostly concentrating in the perinuclear region of the cell (Hagemeijer et al., 2011). As it is unknown what these punctate structures are, we decided to characterize them in more detail. We first investigated whether the $nsp3_C$ and nsp4 puncta co-localize with specific organelle protein markers such as PDI (ER), GM130 (*cis*-Golgi), EDEM1 (ER

and EDEMosomes), and LC3 (autophagosomes). Thus, fusion proteins of nsp3$_C$ (nsp3$_C$-GFP) and nsp4 (nsp4-mCherry) of MHV-A59 were expressed in OST7-1 cells, either individually or in combination, using the vTF7-3 expression system, before being processed for immunofluorescence analyses. As shown in Fig. 2, nsp3$_C$ and nsp4 displayed a recticular distribution pattern and colocalized with the ER marker PDI when expressed singly. When the two viral proteins were co-expressed, the reticular staining pattern for

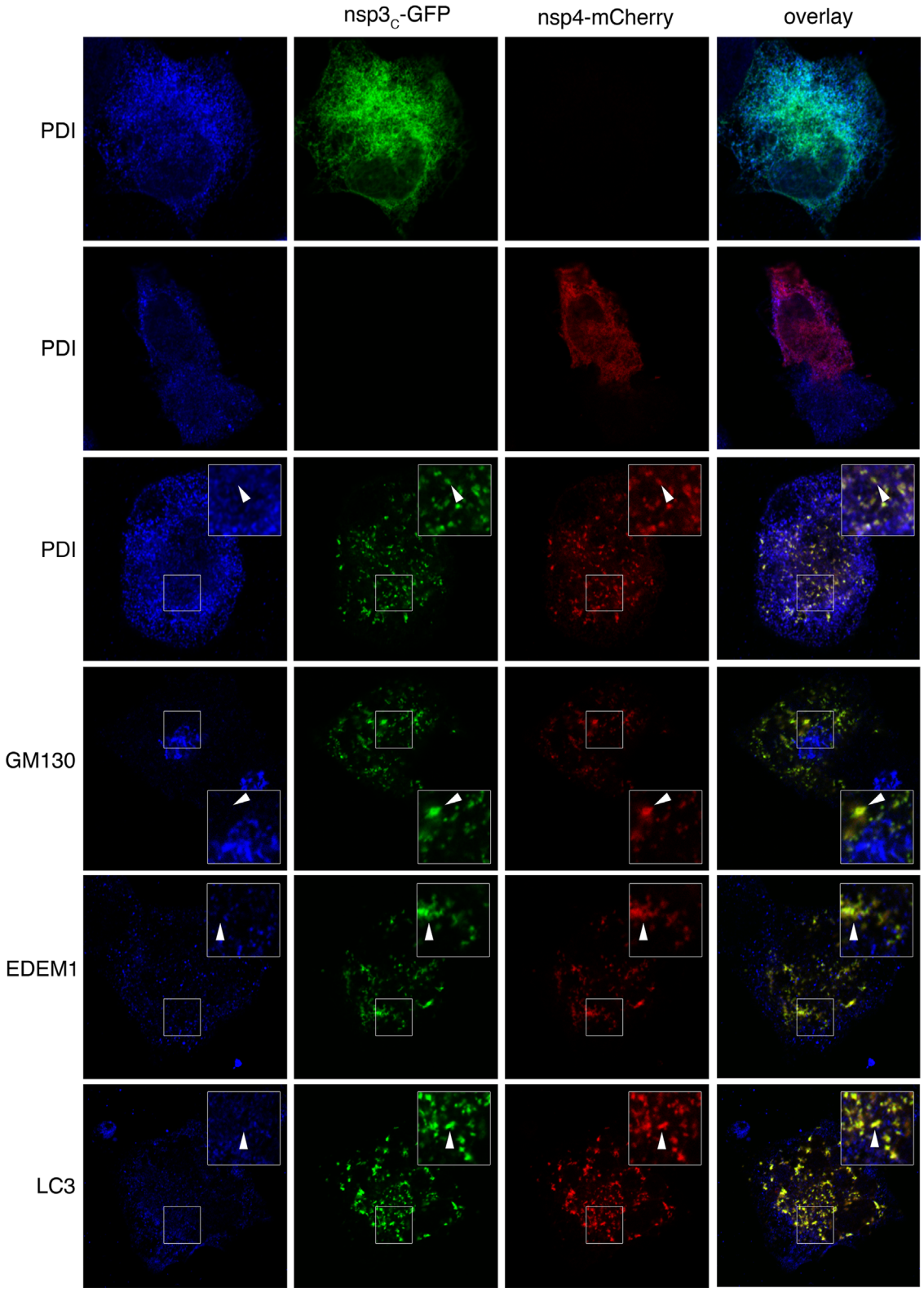

Fig. 2. Analysis of colocalization of cellular markers with nsp3$_C$- and nsp4-positive foci. OST7-1 cells (co)-expressing nsp3$_C$–GFP (green) and/or nsp4-mCherry (red) were stained with antibodies directed either against PDI, GM130, EDEM1, or LC3 (blue). Representative confocal microscopy images are shown.

the viral proteins was no longer apparent, and the two proteins colocalized in discrete perinuclear foci. These foci displayed very little colocalization with the ER marker PDI. Similarly, little (if any) colocalization between these foci and the other tested cellular marker proteins was observed (see insets in Fig. 2).

To characterize the structures to which $nsp3_C$ and nsp4 are associated at the ultrastructural level we performed immuno-electron microscopy (IEM). While mock-transfected cells revealed no labeling (data not shown), specific immuno-gold labeling of the ER was observed when $nsp3_C$-GFP and nsp4-mCherry were individually expressed (Fig. 3A and B) in agreement with previous studies (Oostra et al., 2007; Hagemeijer et al., 2011). When both proteins were co-expressed, the immuno-gold labeling was decorating ER membranes (Fig. 3C and D), which displayed, however, more curvature when compared to the single expressions (compare Fig. 3A′ and B′ with C′ and D′ and see supplementary Fig. S3). To statistically evaluate the membrane curvature induced by co-expression of $nsp3_C$ and nsp4 compared to expression of $nsp3_C$ and nsp4 singly, the gold-labeled ER tubules and cisternae were manually tracked and their relative curvature was determined as detailed in Materials and methods Section and in supplementary Fig. S4. Co-expression of $nsp3_C$-GFP and nsp4-mCherry resulted in significantly more membrane curvature when compared to single expressions of these proteins ($p < 0.01$, *unpaired T-test*). Taken together, from these results we conclude that the discrete foci observed by fluorescence analysis after co-expression of $nsp3_C$ and nsp4 correspond to rearranged ER membranes with increased membrane curvature.

Virus-specific interplay between $nsp3_C$ and nsp4

The discrete foci containing $nsp3_C$ and nsp4 are observed upon co-expression of the two proteins and not when these two proteins are individually expressed. To confirm that the nsp3/nsp4 foci result from a specific interaction between the two proteins, we studied the ability of $nsp3_C$ and nsp4 of MHV-A59 to interact with the corresponding proteins from the SARS-CoV using the fluorescence-lifetime imaging microscopy (FLIM). In contrast to fluorescence resonance energy transfer (FRET) measurements, the FLIM-based FRET measurements are insensitive to the concentration of fluorophores and can thus filter out artifacts introduced by variations in the concentration and emission intensity across the sample. The results in Fig. 4A clearly indicate a specific interaction between $nsp3_C$ and nsp4 when these proteins are from the same virus, in agreement with previous coIP experiments (Hagemeijer et al., 2011). This interaction was not observed when $nsp3_C$ of MHV was co-expressed with nsp4 of SARS-CoV. Co-expression of $nsp3_C$ of SARS-CoV and nsp4 of MHV also resulted in shortening of the fluorescence lifetime, indicative of the two proteins interacting, although less when compared to the cells in which $nsp3_C$ and nsp4 of SARS-CoV were co-expressed. From these results we conclude that only when $nsp3_C$ and nsp4 are from the same virus they are able to efficiently interact with each other.

Next we studied the ability of the MHV-A59 and SARS-CoV $nsp3_C$ and nsp4 fusion proteins to induce the characteristic foci when co-expressed in different combinations. Co-expression of $nsp3_C$ and nsp4 only resulted in the relocalization of these proteins

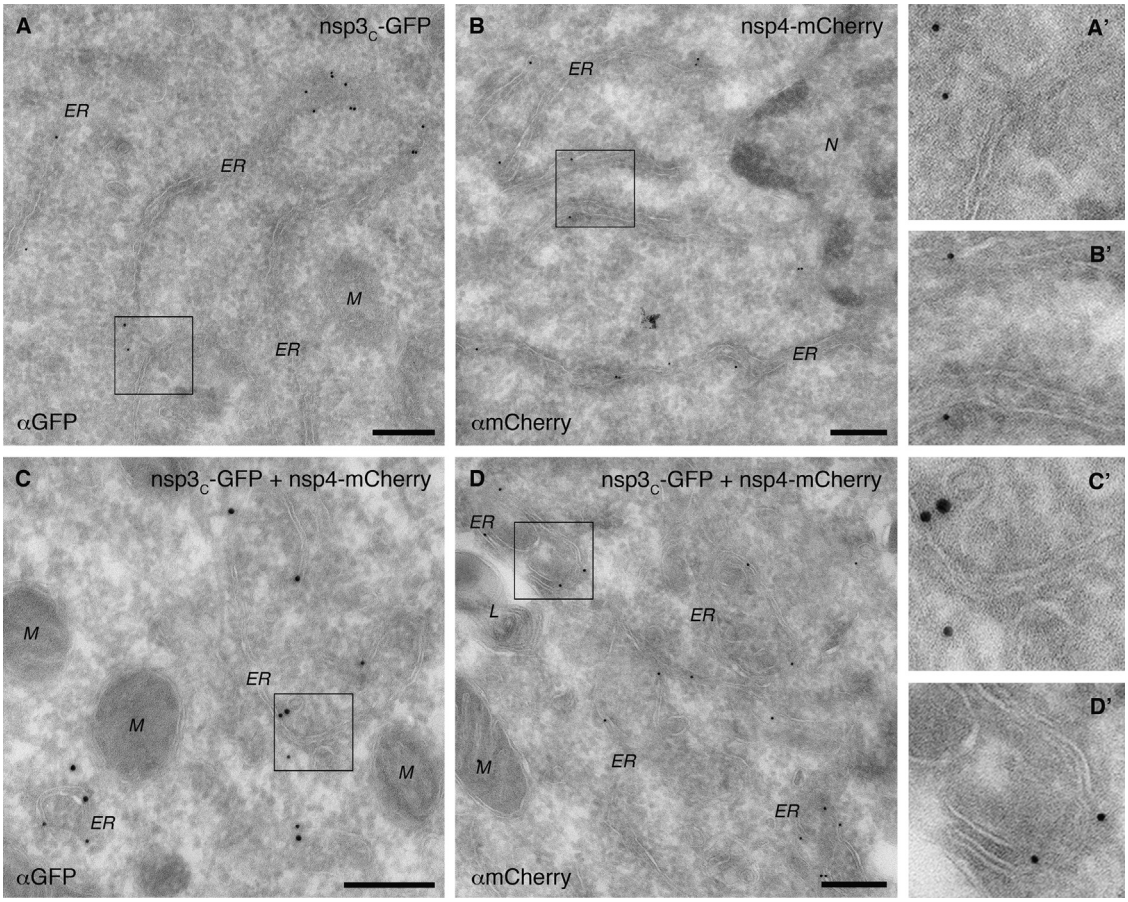

Fig. 3. Immunogold labeling of nsp3C and nsp4 at the induced membrane rearrangements. Immuno-gold labeling of cryo-sections from OST7-1 cells expressing $nsp3_C$-GFP (A and A′), nsp4-mCherry (B and B′) or co-expressing $nsp3_C$–GFP and nsp4-mCherry (C, C′,D and D′). Binding of antibodies directed against the GFP (A, A′, C and C′) or the mCherry (B, B′, D and D′) was visualized by protein A-gold conjugates. ER: endoplasmic reticulum; M: mitochondria; L: lysosome. Scale bar, 200 nm.

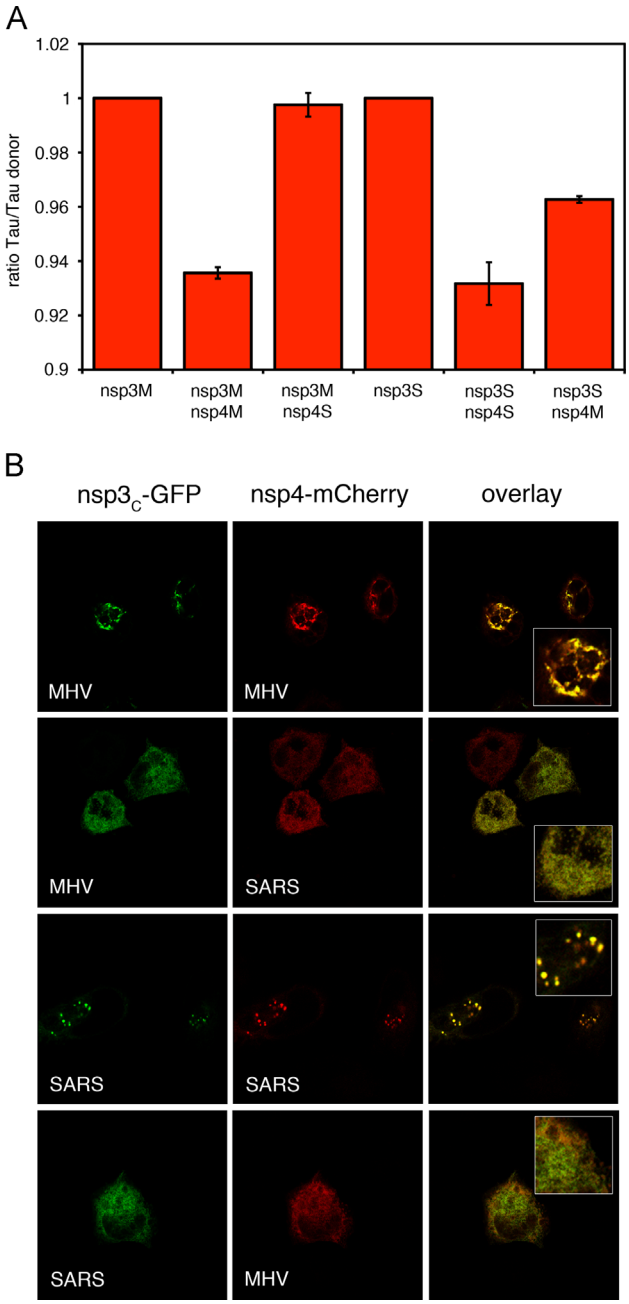

Fig. 4. Nsp3$_C$ and nsp4 interact and induce membrane rearrangements in a virus-specific manner. (A) Fluorescence-lifetime imaging microscopy (FLIM) of OST7-1 cells expressing GFP fusion proteins of nsp3$_C$ (derived either from SARS-CoV [nsp3S] or MHV A59 [nsp3M]) either alone or in combination with mCherry fusion proteins of nsp4 (derived either from SARS-CoV [nsp4S] or MHV A59 [nsp4M]). Fluorescent lifetimes of GFP normalized against the lifetime of GFP when expressed alone are displayed. (B) Nsp3$_C$–GFP and nsp4-mCherry fusion proteins derived from MHV and SARS-CoV were co-expressed in OST7-1 cells in different combinations as indicated. Representative confocal microscopy images are shown.

into the perinuclear foci, when both proteins were from the same virus (Fig. 4B). Quantification of the surface area of the perinuclear foci relative to the surface of the ER showed that MHV and SARS-CoV proteins induced the perinuclear foci to the same extent (26.4% ± 10.7% and 24.8% ± 9.0% surface area of membrane rearrangements relative to ER, respectively) When the nsp3$_C$ and nsp4 proteins of the two different viruses were co-expressed, in both combinations the nsp3$_C$ and nsp4 proteins only displayed the reticular distributions. From these results we conclude that the ability of nsp3$_C$ and nsp4 to redistribute into perinuclear foci is a conserved feature that is observed for different CoVs. Furthermore, a virus-specific interaction between nsp3$_C$ and nsp4 is required as the relocalization is only observed when the two proteins are derived from the same virus.

To gain insights into how the nsp3$_C$/nsp4 complex mediates ER membrane rearrangements, we investigated which part of nsp4 is required for its interplay with nsp3$_C$ by generating hybrid proteins in which the amino-terminal half of nsp4 of MHV-A59 is exchanged by the corresponding region of SARS-CoV nsp4 (designated nsp4$_{SM}$; Fig. 1B). We also constructed plasmids expressing the reciprocal hybrid protein (nsp4$_{MS}$). Co-expression of nsp3$_C$ of MHV-A59 with nsp4$_{MS}$, but not nsp4$_{SM}$, resulted in relocalization of the two proteins from the reticular distribution to the discrete foci (Fig. 5). Similarly for SARS-CoV nsp3$_C$, membrane rearrangements were only observed upon co-expression with nsp4$_{SM}$, but not with nsp4$_{MS}$. The results indicate that the hybrid nsp4 proteins have retained the ability to relocate from the ER to the perinuclear foci when co-expressed with nsp3$_C$ but only when the amino-terminal half of nsp4 is derived from the same CoV species from which nsp3$_C$ is derived. Apparently, the amino-terminal half of nsp4, which includes the large luminal loop (Fig. 1), is a critical determinant for its interplay with nsp3$_C$.

Analysis of deletion mutants of CoV nsp4 and nsp3$_C$

To further study the structural requirements of nsp4 and nsp3$_C$ to induce the perinuclear foci, we analyzed a set of truncated versions of nsp4 and nsp3$_C$ (see Fig. 1C), of which the membrane topology and steady-state expression levels have previously been characterized in detail (Oostra et al., 2008). First, the ability of different nsp4 deletion mutant proteins to induce relocation from the ER to the perinuclear foci was studied (Fig. 6A). All the truncated proteins localized to the ER when individually expressed, similar to the full-length nsp4 protein, as revealed by their reticular distribution (data not shown). Deletion of the carboxy terminus of nsp4, including the fourth transmembrane domain (nsp4 ΔTM4) or both the third and fourth membrane spanning segments (nsp4 ΔTM3-4), did not affect the relocalization of the mutant proteins to the concentrated foci upon co-expression with nsp3$_C$. Additional deletion of the second transmembrane domain (nsp4 ΔTM2-4), which is located immediately downstream of the large luminal loop of nsp4, appeared to affect the relocalization to some extent, as not all nsp3$_C$ and nsp4 proteins relocalized to the concentrated foci; i.e. part of the proteins still displayed the reticular distribution. Nsp4 proteins that also lacked the luminal loop (nsp4 ΔTM2-4+loop) completely lost this ability. An nsp4 deletion mutant lacking the first transmembrane domain and the luminal loop (nsp4 ΔTM1+loop) did also not relocalize upon co-expression with nsp3$_C$. Quantification of the surface area of the perinuclear foci-containing (mutant) nsp4 and nsp3$_C$ relative to the surface area of the ER confirmed these conclusions (supplementary Fig. S4D). In complete agreement with the results obtained with the hybrid nsp4 proteins (Fig. 5), these data revealed that the carboxy-terminal half of nsp4 is dispensable for the induction of the ER-derived membrane rearrangements. Furthermore, the results point to an essential role for the large luminal loop between the first and second transmembrane domain of nsp4.

Next, we analyzed truncated versions of nsp3$_C$, which we have also characterized previously (Oostra et al., 2008). All mutant proteins except one, i.e. nsp3$_C$ ΔTM2+loop (Fig. 1C), displayed the reticular staining pattern characteristic of ER(-associated) proteins when expressed individually (data not shown). In the absence of nsp4, nsp3$_C$ ΔTM2+loop was mainly localized in discrete foci, even though this protein is inserted into the membranes of the ER as evidenced by the addition of N-linked sugars to a C-terminal tag

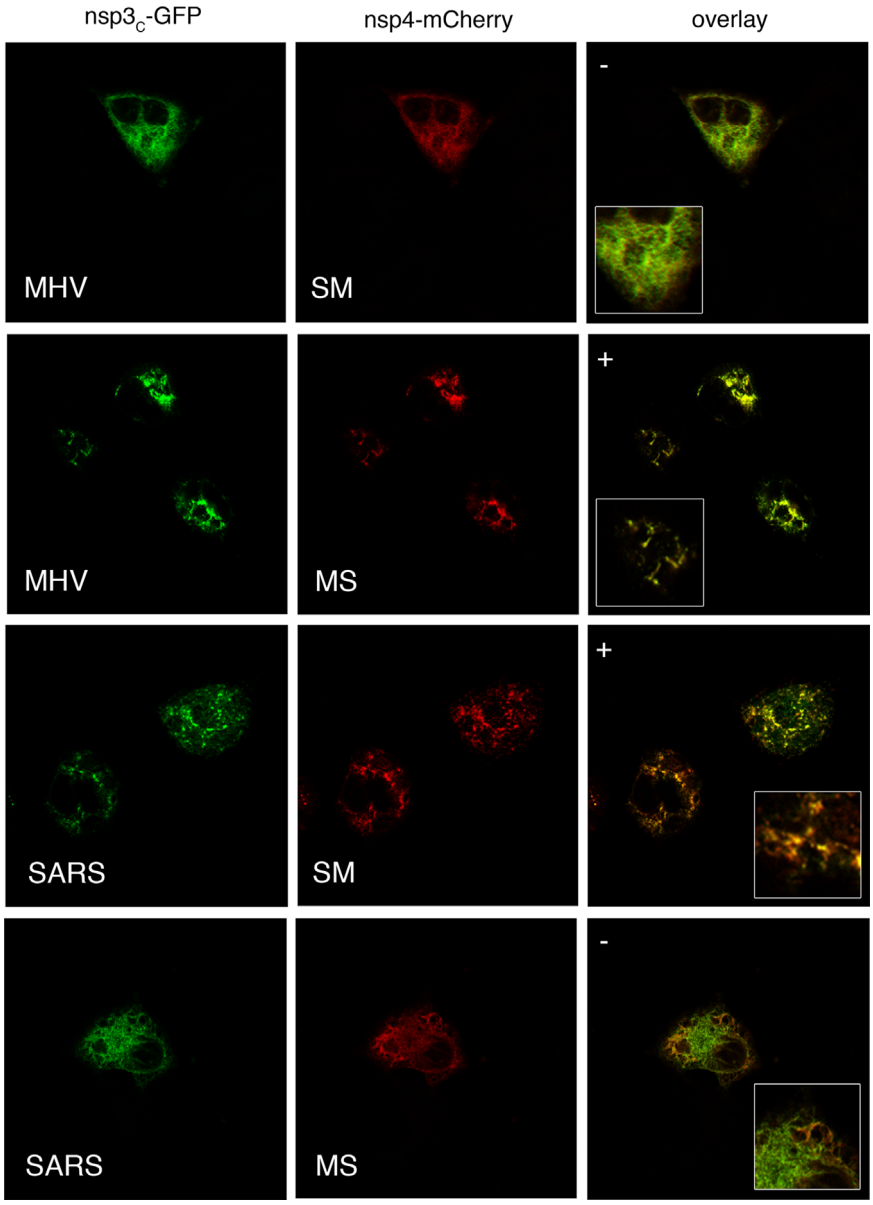

Fig. 5. Induction of membrane rearrangements by nsp3C and nsp4 hybrid proteins. Representative confocal images of OST7-1 cells expressing nsp4-mCherry hybrid proteins (see Fig. 1B) together with nsp3$_C$-GFP derived from either MHV or SARS-CoV. The presence or absence of membrane rearrangements is indicated by the '+' and '−' signs, respectively.

(Oostra et al., 2007). Of the different forms of nsp3 we investigated, nsp3$_C$ was the protein that most efficiently relocalized upon co-expression with nsp4 (Fig. S1). Also nsp3$_C$ ΔTM2 was relocalized to some extent together with nsp4 into discrete foci, although clearly less efficient than nsp3$_C$ as a proportion still displayed the reticular distribution. Additional deletion of the luminal loop completely abrogated the ability of nsp3$_C$ to relocalize together with nsp4. Although this mutant protein (nsp3c ΔTM2+loop) by itself already localized into discrete foci, additional expression of nsp4 did not result in recruitment of nsp4 to these foci. Also no relocalization of nsp4 was observed upon co-expression with the smallest nsp3$_C$ deletion mutant (nsp3$_C$ ΔTM1-2). Quantification of the surface area of the perinuclear foci containing (mutant) nsp3$_C$ and nsp4 relative to the surface area of the ER confirmed these conclusions (supplementary Fig. S4E). The data suggest that the large luminal loop of nsp3 is important for the membrane rearrangements triggered in conjunction with nsp4. Similar to nsp4, the transmembrane domain immediately downstream of the large luminal loop contributes to the relocalization of the nsps, although it is not absolutely essential.

Analysis of the importance of disulfide bridge formation

The large luminal loops of nsp3$_C$ and nsp4 contain four and ten cysteine residues, respectively (indicated in Fig. 1A), which are conserved among the CoVs. The conservation of these residues in nsp3 and nsp4 suggests an important role for the formation of intra-and/or intermolecular disulfide bridges in the virus life cycle. Therefore, we studied whether this protein modification is important for the nsp3$_C$- and nsp4-induced rearrangement of the cellular membranes. Indeed, substitution of each cysteine residue in the large loop of nsp4 by serine dramatically affected the ability of the nsp4 proteins to become localized in the discrete foci upon co-expression with nsp3$_C$ (Fig. S2), as exemplified by the nsp4 C233S mutation in Fig. 6B.

Recruitment of other nsps to the ER membrane rearrangements

Finally we studied the recruitment of other nsps to the ER membranes rearranged by the concerted action of $nsp3_C$ and nsp4.

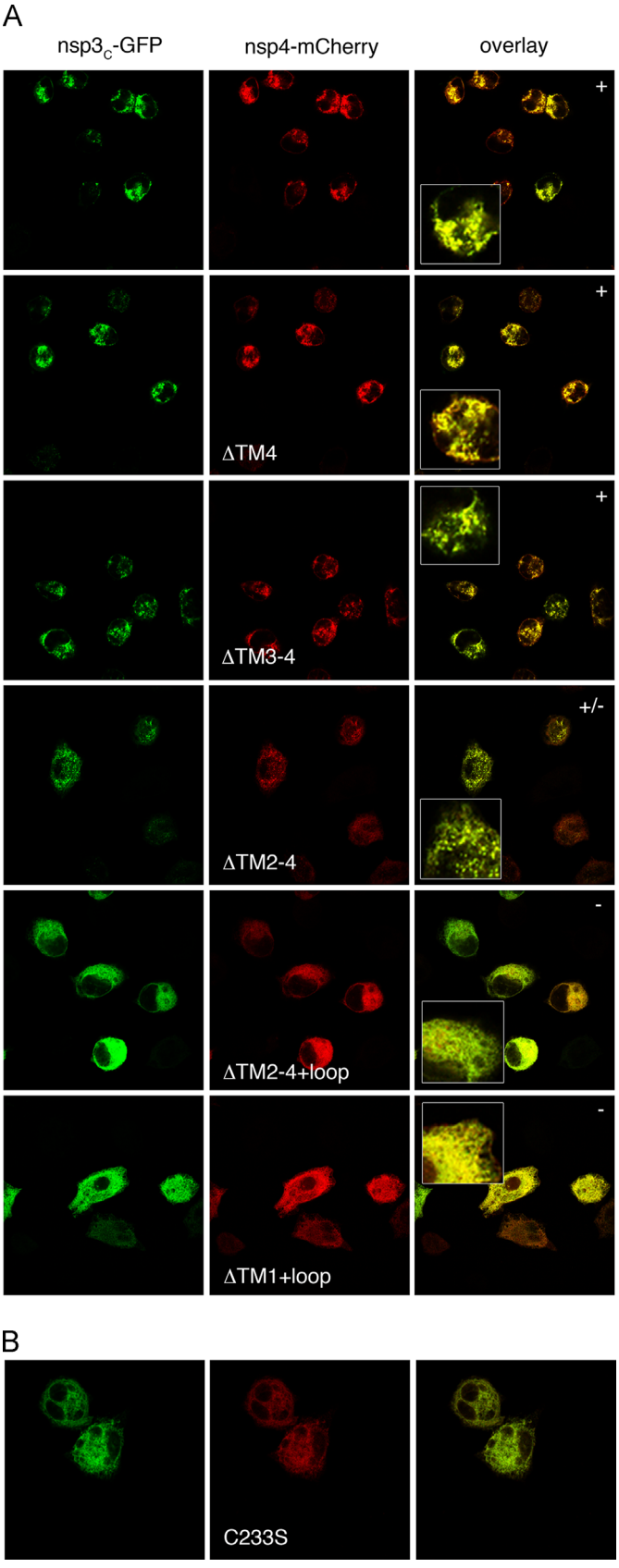

To this end, GFP-tagged versions of all nsps (except the very small nsp11) were co-expressed with nsp4-mCherry and $nsp3_C$–HA. A summary of the results is shown in Fig. 7. Most nsps failed to be recruited to the foci induced by $nsp3_C$ and nsp4, as exemplified in Fig. 7 by nsp14-GFP. However, both nsp2-GFP and nsp6-GFP were found to co-localize with nsp4 and $nsp3_C$. $Nsp3_C$ and nsp4 are thus able to recruit these proteins, possibly through a direct binding, to the rearranged membranes in the absence of other coronaviral components.

Discussion

Upon infection of host cells, CoVs induce a variety of membranous structures (Gosert et al., 2002; Goldsmith et al., 2004; Snijder et al., 2006; Knoops et al., 2008; Ulasli et al., 2010), including the DMVs and CMs that are associated with coronaviral RNA synthesis (van der Meer et al., 1999; Gosert et al., 2002; Hagemeijer et al., 2012b; Maier et al., 2013). Little is known, however, about the mechanism of formation of these structures, in particular about the viral and host proteins implicated in this event. We previously showed that the MHV transmembrane nsps are involved in homo- and heterotypic interactions and that co-expression of the carboxy-terminus of nsp3 ($nsp3_C$) together with nsp4 results in relocalization of these proteins from a recticular distribution representing the ER, into discrete foci often localizing in the perinuclear region of the cell (Hagemeijer et al., 2011). In the present study we reveal that these punctate structures correspond to rearranged ER membranes with increased curvature. The punctate foci were observed upon co-expression of $nsp3_C$ and nsp4 of MHV and of SARS-CoV, but only when the two proteins were derived from the same CoV species. We furthermore show by using a large set of mutant $nsp3_C$ and nsp4 proteins that these ER membrane rearrangements require a specific interplay between $nsp3_C$ and nsp4, which is mostly mediated by their large luminal loops.

Co-expression of $nsp3_C$ and nsp4 results in the induction of ER membrane rearrangements, however the morphology of these structures is not identical to those of the CoV replicative structures, i.e. the DMVs and CMs. Furthermore, colocalization of the cellular marker proteins EDEM1 and LC3, previously shown to be associated with the virus-induced replicative structures (Reggiori et al., 2010), was not observed. Apparently, a full-length nsp3 and/or other viral (nonstructural) proteins are needed for the induction of membrane rearrangements that more closely represent the CoV replicative structures. During the preparation of the current manuscript and in agreement with our conclusion, (Angelini et al., 2013) recently reported that co-expression of full-length nsp3, nsp4 and nsp6 of SARS-CoV is required for the formation of CMs and DMVs, although these DMVs displayed smaller dimensions than those observed in infected cells. Co-transfection of only the SARS-CoV nsp4 and full-length nsp3 resulted in the formation of so-called winding maze-like bodies (Angelini et al., 2013), which appear quite similar to the membrane rearrangements observed after coexpression of $nsp3_C$ and nsp4 of MHV (Fig. 3 and supplementary Fig. S3). Unfortunately, we have not yet been able to clone a functional full-length MHV nsp3 in an expression vector. In contrast to the results of Angelini et al. (2013), others have

Fig. 6. Induction of membrane rearrangements by nsp4 mutant proteins. (A) Full-length and truncated forms of MHV nsp4-mCherry (see Fig. 1C for details) were co-expressed in OST7-1 cells together with MHV $nsp3_C$–GFP. The presence or absence of membrane rearrangements is indicated by the '+' and '−' signs, respectively. '+/−' refers to an intermediate phenotype. (B) Mutant forms of MHV nsp4-mCherry, each carrying a cysteine to serine substitution in the large luminal loop, were analyzed for their ability to induce membrane rearrangements when co-expressed with MHV $nsp3_C$-GFP (Fig. S1). Co-expression of nsp4-mCherry C233S with $nsp3_C$-GFP is shown as representative example.

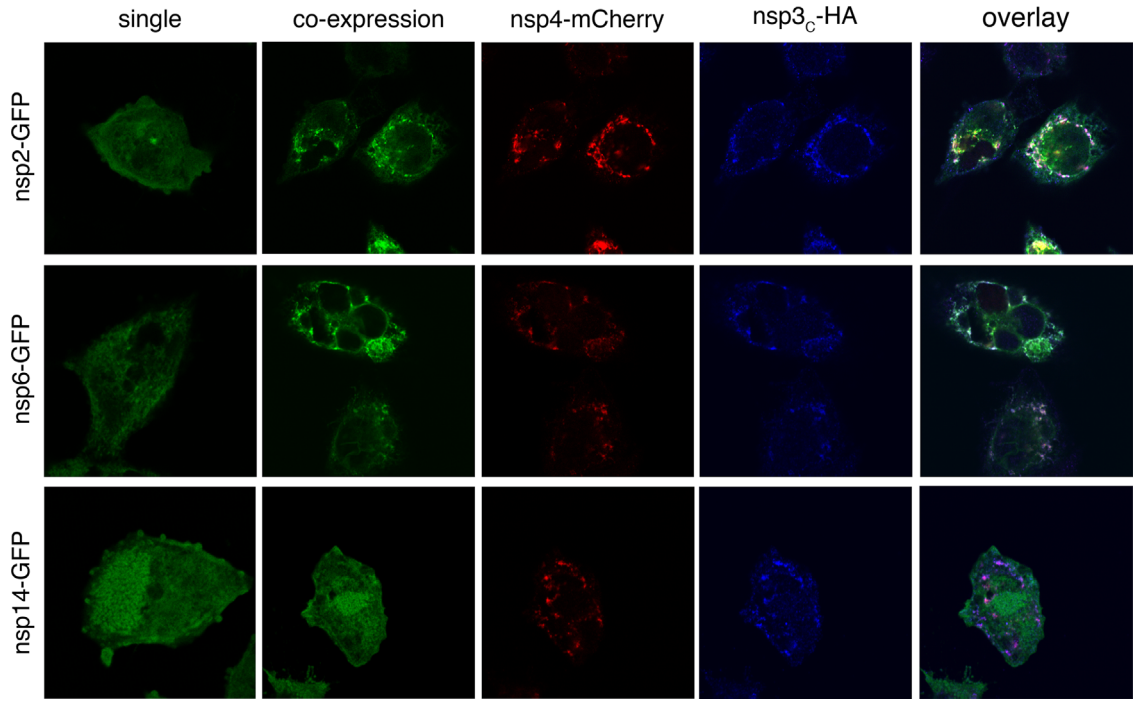

Fig. 7. Recruitment of MHV nsps to the nsp3$_C$- and nsp4-induced membrane rearrangements. GFP-tagged MHV nsp proteins (green) were expressed singly (single) or together (co-expression) with MHV nsp3$_C$-HA (blue) and MHV nsp4-mCherry (red) in OST7-1 cells. Expression of nsp3-HA was visualized using antibodies against the HA tag. Representative confocal images are shown.

previously shown that for the distantly-related equine arteritis virus (EAV, family *Arteriviridae*), co-expression of the full-length arteriviral counterparts of the coronavirus nsp3 and nsp4 proteins (EAV nsp2 and nsp3) is sufficient for the induction of DMVs, although also these structures appeared to differ in size and morphology from those observed in EAV-infected cells (Pedersen et al., 1999; Snijder et al., 2001).

The induction of the perinuclear foci by co-expression of nsp3$_C$ and nsp4 provided a very convenient assay to study the interplay between nsp3$_C$ and nsp4 in more detail. Our results indicate that a specific interplay between nsp3 and nsp4 is required as the perinuclear foci were only observed when the cognate nsp3$_C$ and nsp4 proteins were co-expressed and not when combinations from different viruses were used. The ability of the nsp3$_C$ and nsp4 proteins to induce the membrane rearrangements correlates with the ability of these proteins to interact as demonstrated by the FLIM analyses, in agreement with our previous co-immunoprecipitation studies (Hagemeijer et al., 2011). The specific interplay between nsp3$_C$ and nsp4 was subsequently mapped to the amino-terminal half of nsp4 by using SARS-CoV/MHV-A59 nsp4 hybrids. The hybrid proteins were functional and able to induce membrane rearrangements, but only when their amino-terminal half, which primarily consists of the large luminal loop between the first and second transmembrane domains, was derived from the same CoV species from which nsp3$_C$ was derived.

The importance of the luminal loop between the first and second transmembrane domains of nsp4 for the ER membrane rearrangements was confirmed by a truncation analysis of nsp4. Likewise, the large luminal loop between the first and second transmembrane domain of nsp3 also appears to be of critical importance. Furthermore, although the second transmembrane domain of nsp3$_C$ and nsp4 did not appear to be absolutely essential for the membrane rearrangements, they each promote the induction thereof possibly by facilitating the correct conformation of the luminal loops. In agreement with these results, mutation of each of the ten conserved cysteine residues in the large luminal loop of nsp4 severely affected the ability of this protein to rearrange the ER membranes when co-expressed with nsp3$_C$. Furthermore, treatment of cells with the reducing agent DTT also reduced the number of cells that displayed rearranged membranes (data not shown). The conserved cysteine residues might be important for the interaction between the nsp3 and nsp4 proteins by forming disulfide bridges and/or by mediating the correct folding of the loops. Preliminary data indicate that the interaction between nsp3$_C$ and nsp4 is not governed by the formation of intermolecular disulfide bridges (C.A.M. de Haan and M.C. Hagemeijer; unpublished data), thereby indicating a role for the cysteine residues in mediating the correct folding of the luminal loops.

The CoV transmembrane nsps are probably not only required for the biogenesis of the replicative structures in virus-infected cells, but are likely also involved in anchoring of other nsps to these membranous structures. In agreement with this hypothesis, we show that the membranes rearranged by expression of nsp3$_C$ and nsp4 can recruit the cytosolic nsp2 and the integral membrane protein nsp6. These results are in agreement with previous studies, which show that nsp2 is efficiently recruited to the replicative structures observed in virus-infected cells (Hagemeijer et al., 2010) and that nsp6 interacts with nsp4 (Hagemeijer et al., 2011). The lack of recruitment of other nsps may result from expressing only the C-terminal part of nsp3, as the amino-terminal two-thirds of this protein has been implicated in interactions with multiple other nsps (von Brunn et al., 2007; Imbert et al., 2008; Pan et al., 2008). Alternatively, some proteins may only be recruited when they are part of larger precursor replicase proteins or via interaction with nsp2 and/or nsp6, which in turn are binding nsp3 and/or nsp4.

Taken together, based on the results of us and others, we propose a model in which the interaction between the luminal loops of nsp3 and nsp4 mediate membrane rearrangements by a so-called 'zippering' mechanism (Fig. 8), which generates a membranous anchoring platform able to attract other nsps for the assembly of the CoV RTCs and the subsequent synthesis of CoV RNA.

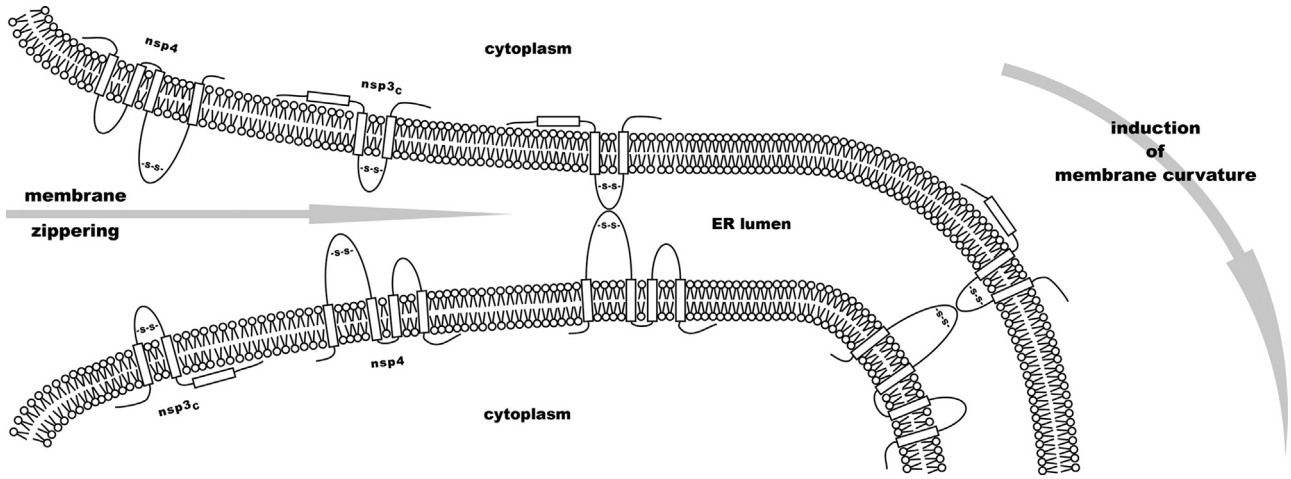

Fig. 8. Model for the interplay between nsp3 and nsp4 in the formation of the CoV replicative structures. The rearrangement of cellular membranes into CoV replicative structures requires the concerted action of both viral and host proteins. We propose that among others the virus contributes to these rearrangements via the expression of nsp3 and nsp4, which interact via their large luminal loops. This interaction "zippers" the ER membranes and induces membrane curvature, two likely requirements for the formation of DMVs that are observed in CoV-infected cells.

Materials and methods

Cells, viruses and antibodies

OST7-1 cells (Elroy-Stein and Moss, 1990) were maintained at 37 °C/5% CO_2 as monolayer cultures in Dulbecco's modified Eagle's medium (DMEM−/−; Cambrex BioScience) containing 10% fetal calf serum (FCS; Bodinco BV), 100 IU/ml of penicillin and 100 μg/ml of streptomycin (both from Life Technologies; referred to as DMEM+/+). The recombinant vaccinia virus encoding the bacteriophage T7 RNA polymerase [vTF7-3; (Fuerst et al., 1986)] was propagated in OST7-1 cells. Antibodies directed against protein-disulfide isomerase [PDI; (Otsu et al., 1994)], GM130 (Becton Dickinson), microtubule-associated protein light chain 3 (LC3; NanoTools), ER degradation-enhancing alpha-mannosidase-like 1 (EDEM1; Sigma) were used to specifically visualize different subcellular structures. Antibodies directed against the hemagglutinin (HA) tag were purchased from Immunology Consultants Laboratory, Inc. (ICL). Antibodies against the enhanced green fluorescent protein (GFP) were obtained from Abcam (Cambridge, United Kingdom) for immuno-electron microscopy studies. Antibodies directed against the mCherry tag were a kind gift of Peter van der Sluijs (Department of Cell Biology, University Medical Center Utrecht, The Netherlands). The antibody against mCherry was generated by injecting rabbits with recombinant GST-mCherry purified from *E. coli*, which had been transformed with pGEX4T3 vector containing the cDNA encoding mCherry. Cy5-conjugated anti-rabbit or anti-mouse secondary antibodies were derived from Jackson Laboratories.

Plasmids

Expression vectors containing the nsp3, nsp4 and nsp6 gene fragments of MHV and SARS-CoV, in frame with sequences coding for GFP, mCherry or the HA tag, under the control of a T7 transcription-regulatory element (Vennema et al., 1991) have been described previously (Oostra et al., 2007, 2008; Hagemeijer et al., 2011). While cDNAs encoding the complete nsp4 protein was used, for nsp3 only the 3'-terminal 2 kb sequence, which encodes all the hydrophobic domains, was cloned ($nsp3_C$; see Fig. 1) (Oostra et al., 2008). Expression vectors containing gene fragments encoding other MHV nsps in frame with the GFP-encoding sequence under the control of a T7 transcription-regulatory element (Vennema et al., 1991) were generated similarly as described previously (Oostra et al., 2007, 2008; Hagemeijer et al., 2010). The MHV-A59 and SARS-CoV nsp4 hybrid protein encoding genes (see Fig. 1) were generated by conventional cloning after performing site-directed mutagenesis on pGEM-$nsp4_S$ (Oostra et al., 2008) [pGEM-$nsp4_{SARS}$-SDM] to introduce a BsmI restriction site in this plasmid. The resulting plasmid was cut using EcorV and BsmI to isolate the gene fragment encoding the amino-terminal half of the SARS-CoV nsp4, followed by ligation of this fragment into pTUG $nsp4_M$-mCherry (Hagemeijer et al., 2011), which was digested with XhoI-followed by a Klenow fill-in reaction- and BsmI, thereby creating pTUG-$nsp4_{SM}$-mCherry. pTUG-$nsp4_{MS}$-mCherry was generated by exchanging the BsmI and BamHI gene fragment in pTUG-$nsp4_{MHV}$-mCherry with that from pGEM-$nsp4_{SARS}$-SDM. Generation of plasmids encoding deletion mutant proteins of nsp4 and $nsp3_C$ or variants thereof fused to GFP has been described previously (Oostra et al., 2008). When indicated the sequence encoding the GFP in these constructs was exchanged with a mCherry-encoding sequence. Plasmids encoding nsp4 in which the cysteine residues were substituted by serine residues were generated by site-directed mutagenesis using appropriate primers using the Quikchange XL site directed mutagenesis kit from Agilent Technologies according to the manufacturer's instructions. All plasmids were confirmed by sequencing. In Fig. 1B and C a schematic overview of all $nsp3_C$ and nsp4 constructs that were used in this study is given.

Infection and transfection

Subconfluent monolayers of OST7-1 cells were grown in 2-cm^2 tissue culture dishes and inoculated with vTF7-3 at a multiplicity of infection (MOI) of 10. Cells were transfected 1 h after infection by incubation of the cells for 5 min with a transfection mixture consisting of 100 μl DMEM−/−, 2 μl Lipofectin (Invitrogen) and 1 μg of each selected plasmid, after which another 200 μl DMEM−/− was added. At 3 h post infection (p.i.), the transfection mixture was replaced by DMEM+/+ until further processing.

Immunofluorescence microscopy

OST7-1 cells grown on glass coverslips were fixed using a 4% paraformadehyde solution in phosphate-buffered saline (PBS) for 30 min at room temperature at 5 or 6 h p.i. After washing the cover slips once with PBS, the cells were permeabilized using 0.1% Triton X-100 for 10 min at room temperature, followed by a 15 min incubation in blocking buffer (PBS containing 10% normal goat

serum). Subsequently, the cells were incubated for 45 min with the indicated primary antibodies. After three washes with PBS, the cells were incubated for 45 min with Cy5-conjugated secondary antibodies, followed by three washing steps with PBS, one time rinsing with water and embedding of the cover slips using FluorSave (Calbiochem). The samples were examined using a Leica TCS SP fluorescent confocal microscope. The surface area of the highly fluorescent perinuclear foci and of the ER (including the perinuclear foci) was quantified using Image J (Rasband and ImageJ, 1997-2014) by manually applying a threshold. For each experimental condition, 5–10 cells were quantified.

Immuno-electron microscopy

From 2 h p.i. onwards, the vTF7-3 infected cells were treated with 5 mM hydroxyurea to prevent vaccinia virus DNA synthesis. This treatment did not affect expression of the nsps or their relocalization as analyzed by immunofluorescence microscopy. At 6 h p.i., the infected and (co)-transfected OST7-1 cells were processed for immuno-electron microscopy (IEM) as previously described (Hagemeijer et al., 2010; Ulasli et al., 2010; Verheije et al., 2010). The nsp3$_C$-GFP construct was visualized using antibodies against the GFP, whereas the nsp4-mCherry fusion protein was detected using antibodies against mCherry. Protein A-gold conjugates were prepared following an established protocol (Slot and Geuze, 2007). Sections were viewed in a JEOL 1010 or a JEOL 1200 electron microscope (JEOL, Tokyo, Japan) and images were recorded on Kodak 4489 sheet films (Kodak, Rochester, NY). No labeling was observed in mock-transfected cells. ER tubules/cisternae in the IEM pictures decorated with anti-GFP and/or anti-mCherry antibodies were manually tracked ($n=60$). The ends of the resulting tracks were horizontally aligned and boxed. The ratio of the width and length of each box, which is a measure for the curvature of the line, was determined. This ratio is small for a nearly linear line and increases with increased curvature ((with a maximum value$=1$); see supplementary Fig. S4A and B).

Fluorescence-lifetime imaging microscopy (FLIM)

Determination of fluorescence lifetime was done as previously described (Hofman et al., 2008). Cells were transfected with the indicated constructs and subsequently lifetime of GFP was determined using a Nikon PCM 2000 CSLM equipped with a fluorescence lifetime module (LiMo, Nikon), which captures four images in four consecutive time gates of approximately 2 ns each. The excitation light was provided by a frequency doubled picoseconds pulsed Ti:Sa laser (Tsunami, Spectra Physics). For imaging a NA$=1.20/40x$ water emission objective and the medium-sized pinhole were used. The four-gate intensity decays recorded for each pixel were fitted with a monoexponential decay using the LiMO software, meaning that also for probes with multiexponential decays, one single average lifetime is observed. Lifetimes described in this study should therefore be considered as average lifetimes. Intensity thresholding was performed to remove background-(glass) and auto-fluorescence. To rule out effects of cell-to-cell variation in FRET efficiency, lifetimes of at least four cells were determined and a student T-test was performed to determine statistical significances. Fluorescent lifetimes were normalized against the lifetime of GFP alone.

Acknowledgments

We would like to thank Oliver Wicht and Christine Burkhard from the Virology Division, Faculty of Veterinary Medicine, Utrecht University and Fleur de Haan for suggestions and stimulating discussions. C.A.M.D.H. is supported by Grants from the Netherlands Organization for Scientific Research (NWO-ALW; 819.02.023) and Utrecht University (High Potential). F.R. is supported by ECHO (700.59.003), ALW Open Program (821.02.017) and DFG-NWO cooperation (DN82-303/UN111/7-1) Grants. The funding sources had no involvement in the collection, analysis and interpretation of the data, the writing of the report and the decision to submit the article for publication.

Appendix A. Supporting information

Supplementary data associated with this article can be found in the online version at http://dx.doi.org/10.1016/j.virol.2014.04.027.

References

Altan-Bonnet, N., Balla, T., 2012. Phosphatidylinositol 4-kinases: hostages harnessed to build panviral replication platforms. Trends Biochem. Sci. 37, 293–302.
Angelini, M.M., Akhlaghpour, M., Neuman, B.W., Buchmeier, M.J., 2013. Severe acute respiratory syndrome coronavirus nonstructural proteins 3, 4, and 6 induce double-membrane vesicles. mBio 4, pii: e00524–13.
Baliji, S., Cammer, S.A., Sobral, B., Baker, S.C., 2009. Detection of nonstructural protein 6 in murine coronavirus-infected cells and analysis of the transmembrane topology by using bioinformatics and molecular approaches. J. Virol. 83, 6957–6962.
Belov, G.A., van Kuppeveld, F.J., 2012. (+)RNA viruses rewire cellular pathways to build replication organelles. Curr. Opin. Virol. 2, 740–747.
Bernasconi, R., Galli, C., Noack, J., Bianchi, S., de Haan, C.A., Reggiori, F., Molinari, M., 2012. Role of the SEL1L:LC3-I complex as an ERAD tuning receptor in the mammalian ER. Mol. Cell. 46, 809–819.
de Wilde, A.H., Raj, V.S., Oudshoorn, D., Bestebroer, T.M., van Nieuwkoop, S., Limpens, R.W., et al., 2013. MERS-coronavirus replication induces severe in vitro cytopathology and is strongly inhibited by cyclosporin A or interferon-alpha treatment. J. Gen. Virol. 94, 1749–1760.
Delang, L., Paeshuyse, J., Neyts, J., 2012. The role of phosphatidylinositol 4-kinases and phosphatidylinositol 4-phosphate during viral replication. Biochem. Pharmacol. 84, 1400–1408.
Deming, D.J., Graham, R.L., Denison, M.R., Baric, R.S., 2007. Processing of open reading frame 1a replicase proteins nsp7 to nsp10 in murine hepatitis virus strain A59 replication. J. Virol. 81, 10280–10291.
den Boon, J.A., Ahlquist, P., 2010a. Organelle-like membrane compartmentalization of positive-strand RNA virus replication factories. Annu. Rev. Microbiol. 64, 241–256.
den Boon, J.A., Diaz, A., Ahlquist, P., 2010b. Cytoplasmic viral replication complexes. Cell Host Microbe. 8, 77–85.
Elroy-Stein, O., Moss, B., 1990. Cytoplasmic expression system based on constitutive synthesis of bacteriophage T7 RNA polymerase in mammalian cells. Proc. Natl. Acad. Sci. USA 87, 6743–6747.
Fuerst, T.R., Niles, E.G., Studier, F.W., Moss, B., 1986. Eukaryotic transient-expression system based on recombinant vaccinia virus that synthesizes bacteriophage T7 RNA polymerase. Proc. Natl. Acad. Sci. USA 83, 8122–8126.
Gadlage, M.J., Sparks, J.S., Beachboard, D.C., Cox, R.G., Doyle, J.D., Stobart, C.C., Denison, M.R., 2010. Murine hepatitis virus nonstructural protein 4 regulates virus-induced membrane modifications and replication complex function. J. Virol. 84, 280–290.
Goldsmith, C.S., Tatti, K.M., Ksiazek, T.G., Rollin, P.E., Comer, J.A., Lee, W.W., et al., 2004. Ultrastructural characterization of SARS coronavirus. Emerg. Infect. Dis. 10, 320–326.
Gorbalenya, A.E., Enjuanes, L., Ziebuhr, J., Snijder, E.J., 2006. Nidovirales: evolving the largest RNA virus genome. Virus Res. 117, 17–37.
Gosert, R., Kanjanahaluethai, A., Egger, D., Bienz, K., Baker, S.C., 2002. RNA replication of mouse hepatitis virus takes place at double-membrane vesicles. J. Virol. 76, 3697–3708.
Graham, R.L., Sims, A.C., Brockway, S.M., Baric, R.S., Denison, M.R., 2005. The nsp2 replicase proteins of murine hepatitis virus and severe acute respiratory syndrome coronavirus are dispensable for viral replication. J. Virol. 79, 13399–13411.
Hagemeijer, M.C., Rottier, P.J., de Haan, C.A., 2012a. Biogenesis and dynamics of the coronavirus replicative structures. Viruses 4, 3245–3269.
Hagemeijer, M.C., Ulasli, M., Vonk, A.M., Reggiori, F., Rottier, P.J., de Haan, C.A., 2011. Mobility and interactions of coronavirus nonstructural protein 4. J. Virol. 85, 4572–4577.
Hagemeijer, M.C., Verheije, M.H., Ulasli, M., Shaltiel, I.A., de Vries, L.A., Reggiori, F., et al., 2010. Dynamics of coronavirus replication–transcription complexes. J. Virol. 84, 2134–2149.
Hagemeijer, M.C., Vonk, A.M., Monastyrska, I., Rottier, P.J., de Haan, C.A., 2012b. Visualizing coronavirus RNA synthesis in time by using click chemistry. J. Virol. 86, 5808–5816.

Harcourt, B.H., Jukneliene, D., Kanjanahaluethai, A., Bechill, J., Severson, K.M., Smith, C.M., et al., 2004. Identification of severe acute respiratory syndrome coronavirus replicase products and characterization of papain-like protease activity. J. Virol. 78, 13600–13612.

Hofman, E.G., Ruonala, M.O., Bader, A.N., van den Heuvel, D., Voortman, J., Roovers, R.C., et al., 2008. EGF induces coalescence of different lipid rafts. J. Cell Sci. 121, 2519–2528.

Imbert, I., Snijder, E.J., Dimitrova, M., Guillemot, J.C., Lecine, P., Canard, B., 2008. The SARS-Coronavirus PLnc domain of nsp3 as a replication/transcription scaffolding protein. Virus Res. 133, 136–148.

Kanjanahaluethai, A., Chen, Z., Jukneliene, D., Baker, S.C., 2007. Membrane topology of murine coronavirus replicase nonstructural protein 3. Virology 361, 391–401.

Knoops, K., Kikkert, M., Worm, S.H., Zevenhoven-Dobbe, J.C., van der Meer, Y., Koster, A.J., et al., 2008. SARS-coronavirus replication is supported by a reticulovesicular network of modified endoplasmic reticulum. PLoS Biol. 6, e226.

Maier, H.J., Hawes, P.C., Cottam, E.M., Mantell, J., Verkade, P., Monaghan, P., et al., 2013. Infectious bronchitis virus generates spherules from zippered endoplasmic reticulum membranes. mBio 4.

Miller, S., Krijnse-Locker, J., 2008. Modification of intracellular membrane structures for virus replication. Nat. Rev. Microbiol. 6, 363–374.

Oostra, M., Hagemeijer, M.C., van Gent, M., Bekker, C.P., te Lintelo, E.G., Rottier, P.J., de Haan, C.A., 2008. Topology and membrane anchoring of the coronavirus replication complex: not all hydrophobic domains of nsp3 and nsp6 are membrane spanning. J. Virol. 82, 12392–12405.

Oostra, M., te Lintelo, E.G., Deijs, M., Verheije, M.H., Rottier, P.J., de Haan, C.A., 2007. Localization and membrane topology of coronavirus nonstructural protein 4: involvement of the early secretory pathway in replication. J. Virol. 81, 12323–12336.

Otsu, M., Omura, F., Yoshimori, T., Kikuchi, M., 1994. Protein disulfide isomerase associates with misfolded human lysozyme in vivo. J. Biol. Chem. 269, 6874–6877.

Pan, J., Peng, X., Gao, Y., Li, Z., Lu, X., Chen, Y., et al., 2008. Genome-wide analysis of protein–protein interactions and involvement of viral proteins in SARS-CoV replication. PloS One 3, e3299.

Pedersen, K.W., van der Meer, Y., Roos, N., Snijder, E.J., 1999. Open reading frame 1a-encoded subunits of the arterivirus replicase induce endoplasmic reticulum-derived double-membrane vesicles which carry the viral replication complex. J. Virol. 73, 2016–2026.

Prentice, E., McAuliffe, J., Lu, X., Subbarao, K., Denison, M.R., 2004. Identification and characterization of severe acute respiratory syndrome coronavirus replicase proteins. J. Virol. 78, 9977–9986.

Rasband, W.S., 1997–2014. ImageJ, U.S. National Institutes of Health. Bethesda, Maryland, USA ⟨http://imagej.nih.gov/ij/⟩.

Reggiori, F., Monastyrska, I., Verheije, M.H., Cali, T., Ulasli, M., Bianchi, S., et al., 2010. Coronaviruses Hijack the LC3-I-positive EDEMosomes, ER-derived vesicles exporting short-lived ERAD regulators, for replication. Cell Host Microbe 7, 500–508.

Shi, S.T., Schiller, J.J., Kanjanahaluethai, A., Baker, S.C., Oh, J.W., Lai, M.M., 1999. Colocalization and membrane association of murine hepatitis virus gene 1 products and De novo-synthesized viral RNA in infected cells. J. Virol. 73, 5957–5969.

Slot, J.W., Geuze, H.J., 2007. Cryosectioning and immunolabeling. Nat. Protoc. 2, 2480–2491.

Snijder, E.J., van der Meer, Y., Zevenhoven-Dobbe, J., Onderwater, J.J., van der Meulen, J., Koerten, H.K., Mommaas, A.M., 2006. Ultrastructure and origin of membrane vesicles associated with the severe acute respiratory syndrome coronavirus replication complex. J. Virol. 80, 5927–5940.

Snijder, E.J., van Tol, H., Roos, N., Pedersen, K.W., 2001. Non-structural proteins 2 and 3 interact to modify host cell membranes during the formation of the arterivirus replication complex. J. Gen. Virol. 82, 985–994.

Sparks, J.S., Lu, X., Denison, M.R., 2007. Genetic analysis of Murine hepatitis virus nsp4 in virus replication. J. Virol. 81, 12554–12563.

Ulasli, M., Verheije, M.H., de Haan, C.A., Reggiori, F., 2010. Qualitative and quantitative ultrastructural analysis of the membrane rearrangements induced by coronavirus. Cell Microbiol. 12, 844–861.

van der Meer, Y., Snijder, E.J., Dobbe, J.C., Schleich, S., Denison, M.R., Spaan, W.J., Locker, J.K., 1999. Localization of mouse hepatitis virus nonstructural proteins and RNA synthesis indicates a role for late endosomes in viral replication. J. Virol. 73, 7641–7657.

Vennema, H., Rijnbrand, R., Heijnen, L., Horzinek, M.C., Spaan, W.J., 1991. Enhancement of the vaccinia virus/phage T7 RNA polymerase expression system using encephalomyocarditis virus 5'-untranslated region sequences. Gene 108, 201–209.

Verheije, M.H., Hagemeijer, M.C., Ulasli, M., Reggiori, F., Rottier, P.J., Masters, P.S., de Haan, C.A., 2010. The coronavirus nucleocapsid protein is dynamically associated with the replication–transcription complexes. J. Virol. 84, 11575–11579.

von Brunn, A., Teepe, C., Simpson, J.C., Pepperkok, R., Friedel, C.C., Zimmer, R., et al., 2007. Analysis of intraviral protein–protein interactions of the SARS coronavirus ORFeome. PloS one 2, e459.